Soft Matter

Accepted Manuscript

This is an *Accepted Manuscript*, which has been through the Royal Society of Chemistry peer review process and has been accepted for publication.

Accepted Manuscripts are published online shortly after acceptance, before technical editing, formatting and proof reading. Using this free service, authors can make their results available to the community, in citable form, before we publish the edited article. We will replace this *Accepted Manuscript* with the edited and formatted *Advance Article* as soon as it is available.

You can find more information about *Accepted Manuscripts* in the **Information for Authors**.

Please note that technical editing may introduce minor changes to the text and/or graphics, which may alter content. The journal's standard **Terms & Conditions** and the **Ethical guidelines** still apply. In no event shall the Royal Society of Chemistry be held responsible for any errors or omissions in this *Accepted Manuscript* or any consequences arising from the use of any information it contains.

β-Lactoglobulin nanofibrils can be assembled into nanotapes via site-specific interactions with pectin†

Charith A. Hettiarachchi,[ab] Laurence D. Melton,[*ab] Duncan J. McGillivray,[abc] Simon M. Loveday,[ad] Juliet A. Gerrard,[abcef] and Martin A. K. Williams[acg]

[a]Riddet Institute, Massey University, Private Bag 11222, Palmerston North 4442, New Zealand

[b]School of Chemical Sciences, University of Auckland, Private Bag 92019, Auckland 1142, New Zealand. E-mail: l.melton@auckland.ac.nz; Tel: +64 9 3737 599 ext. 86658

[c]MacDiarmid Institute for Advanced Materials and Nanotechnology, Wellington 6140, New Zealand

[d]Massey Institute of Food Science and Technology, Massey University, Private Bag 11222, Palmerston North 4442, New Zealand

[e]School of Biological Sciences, University of Auckland, Private Bag 92019, Auckland 1142, New Zealand

[f]Callaghan Innovation, PO Box 31310, Lower Hutt 5040, New Zealand

[g]Institute of Fundamental Sciences, Massey University, Private Bag 11222, Palmerston North 4442, New Zealand

1

Table of content entry

A β-lactoglobulin nanotape

β-Lactoglobulin nanofibrils — Pectin molecules
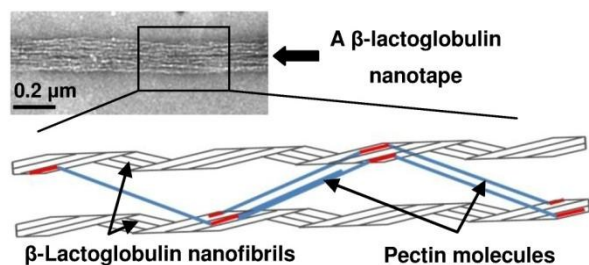
Abstract

Controlling the self- assembly of individual supramolecular entities, such as amyloid fibrils, into hierarchical architectures enables the 'bottom-up' fabrication of useful bionanomaterials. Here, we present the hierarchical assembly of β-lactoglobulin nanofibrils into the form of 'nanotapes' in the presence of a specific pectin with a high degree of methylesterification. The nanotapes produced were highly ordered, and had an average width of 180 nm at pH 3. Increasing the ionic strength or the pH of the medium led to the disassembly of nanotapes, indicating that electrostatic interactions stabilised the nanotape architecture. Small-angle X-ray scattering experiments conducted on the nanotapes showed that adequate space is available between adjacent nanofibrils to accommodate pectin molecules. To locate the interaction sites on the pectin molecule, it was subjected to endopolygalacturonase digestion, and the resulting products were analysed using capillary electrophoresis and size-exclusion chromatography for their charge and molecular weight, respectively. Results suggested that the functional pectin molecules carry short (< 10 residues) enzyme-susceptible blocks of negatively charged, non-methylesterified galacturonic acid residues in the middle of their homogalacturonan backbones (and possibly near their ends), that specifically bind to sites on the nanofibrils. Blocking the interaction sites on the nanofibril surface using small oligomers of non-methylesterified galacturonic acid residues similar in size to the interaction sites of the

pectin molecule decreased the nanotape formation, indicating that site-specific electrostatic interactions are vital for the cross-linking of nanofibrils. We propose a structural model for the pectin-cross-linked β-lactoglobulin nanotapes, the elements of which will inform the future design of bionanomaterials.

Introduction

The self-assembly of biological molecules into functional nanostructures and machines *in vivo*[1–3] and *in vitro*[4,5] has inspired many examples of biomimetic assembly.[6–8] However, beyond those that have evolved in biology,[9,10] there have been strikingly few examples of biomolecules being used to construct useful new nanoarchitectures. Amyloid fibrils are an exception to the rule, as their formation and morphology can be controlled with relative precision,[11–14] and their bionanotechnological potential is increasingly recognised.[15–19] Some peptides and proteins have been found to act as templates to generate extra large amyloid fibrils.[20,21] Yet, gaining control over the assembly of amyloid fibrils remains a challenge, as the mapping of the surface charge distribution has become a complex issue, due to variations in the number and sequence of the amino acid residues in the peptides that assemble into different fibrils.[22,23]

We have investigated the formation of hierarchical architectures from β-lactoglobulin (β-lg) nanofibrils, a type of amyloid fibril, by interacting them with pectins having different degrees of methylesterification (DM).[24] Among them, a pectin with a DM of ~86% was capable of laterally binding the nanofibrils into ordered 'nanotapes' at pH 2 and pH 3. We now present work carried out on the determination of the structure of these nanotapes.

β-Lg, the major protein in the whey fraction of bovine milk, has a compact globular structure rich in β-sheets,[25] and exists effectively as a dimer over the pH range of 2.5 to 7.5.[26] On heating above 75 °C at pH values between 1.6 and 2.4, and at low ionic strength, it is

denatured and partially hydrolysed, and the resulting species readily assemble *via* β-sheet stacking to form amyloid fibrils.[23,27–29]

Heat-induced β-lg nanofibrils are typically composed of 2 to 3 protofilaments that have laterally aligned and twisted along the long axis, giving them an appearance of a twisted ribbon.[30,31] The diameter of a single β-lg protofilament is reported to be ~2 nm, whilst the diameters of β-lg nanofibrils formed by 2 and 3 protofilaments are found to be about 4 and 6 nm, respectively, based on atomic force microscopic (AFM) height measurements.[30] The persistence length (l_p) of these nanofibrils falls within the range 0.6 to 2.5 μm,[11,30,32] and their contour length (l_c) averages around 5 μm, with some extending up to 10 μm.[30,33,34] Given that the l_c of these nanofibrils is comparable to their l_p, they are classified as a type of semi-flexible fibrils.

β-Lg nanofibrils carry a net positive surface charge at pH values below 5,[35,36] due to the presence of lysine, arginine and histidine residues in their component β-strands.[23,29] The availability of hydrophobic regions on the nanofibril surface is evidenced by the affinity of 8-anilino-1-naphthalene sulfonate molecules for the nanofibril surface.[29] The heterogeneous surface on the β-lg nanofibrils presents opportunities for complexing with other biomolecules by ionic or other non-covalent mechanisms.

Pectin is an anionic, plant cell wall polysaccharide that has a backbone mainly consisting of D-galacturonic acid (GalA) residues, with branches composed of neutral sugar residues[37] that originate from short rhamnogalacturonan sections of the backbone. GalA residues in the backbone may exist esterified with methanol, and the percentage of methylesterified GalA residues to the sum of methylesterified and non-methylesterified GalA residues is defined as DM. The lower the DM of a pectin the larger the number of potentially negatively charged groups available on its backbone (at pH values above the pK_a of the carboxylate group), and it is one of the major factors that determines the magnitude of

4

electrostatic interactions between pectin and β-lg nanofibrils.[24] The DM of a pectin can be reduced by pectin methylesterase enzymes or by alkaline treatment,[38,39] and can be increased by reacting with methyliodine or methanolic sulphuric acid.[40,41]

In addition to DM, the distribution of the non-methylesterified GalA residues along the backbone of the pectin molecules will also affect their electrostatic interactions with β-lg nanofibrils. In fact, pectins with either block-wise or random distributions of non-methylesterified GalA residues have already been shown to interact differently with native β-lg.[42,43] Typical methods for the determination of differences in the intra-molecular distributions of non-methylesterified GalA residues between pectins mainly involve using site-specific enzymatic cleavage of pectin backbone followed by analysis of the resulting fragments for their size and charge.[44–46]

Hydrophobic interactions between pectin and β-lg nanofibrils can potentially occur via the methylesterified GalA residues of pectin. However, the strength of hydrophobic interactions is relatively difficult to modulate in a specific and controlled way, because they are influenced by temperature and solvent structure in a non-trivial manner. By contrast, electrostatic interactions can be easily modulated by varying ionic strength and pH of the medium, which influences charge shielding and the dissociation equilibria of ionisable species, respectively. Here, we further demonstrate that the assembly of β-lg nanofibrils into nanotapes via site-specific electrostatic interactions with pectin can be controlled by manipulating the ionic environment.

Experimental

Materials

Lyophilised bovine β-lg, a mixture of variants A and B (L01030) and a high methoxyl citrus

pectin with a GalA content of 88.5% w/w (dry basis) (P9561) were purchased from Sigma (St

Louis, MO, USA). The pectin had an average DM of 86 ± 2% as measured by capillary

electrophoresis (CE),[24] and it was designated DM86. Weight-average molecular weight (M_w)

and number-average molecular weight (M_n) of DM86 were 47.8 ± 2.8 kDa, and 39.3 ± 0.3

kDa, respectively as measured by size exclusion chromatography (SEC) coupled with multi-

angle laser light scattering (MALLS) and refractive index (RI) detectors,[24] giving it a

polydispersity index (PDI) of 1.2. GalA monomer was obtained from Fluka Biochemika

(Steinheim, Germany). A mixture of the sodium salts of GalA heptamers and octamers was

purchased from Eliciyl (Crolles, France). An endopolygalacturonase-II (endo-PG)

concentrate from *Aspergillus niger* was provided by Jacques A. E. Benen, Wageningen

University, The Netherlands. All the chemicals used for the experiments were of analytical

grade or highest available purity. Deionised water with a resistivity of 18.2 MΩ cm was

obtained from an in-house MilliQ filtration system (Billerica, MA, USA) and used throughout

the experiments.

Preparation of β-lg nanofibril samples

β-Lg nanofibrils were formed by both conventional heating and microwave heating of β-lg

solutions at pH 2 as given by Hettiarachchi *et al.*,[29] and they are named CH and MHS,

respectively. The solutions used for the nanofibril formation had β-lg concentrations of 20 and

16 mg mL^{-1}. Aliquots obtained from the nanofibril sample prepared from 20 mg mL^{-1} β-lg

solution were diluted 10-fold with water that had been adjusted to pH 3 with HCl (pH 3 HCl)

and they were centrifuged at ~200 × *g* for 5 min (Heraeus Labofuge 400, Hanau, Germany) to

remove macroscopic aggregates formed during the nanofibril formation.[29] The samples were

then checked for their pH, and adjusted to pH 3 using 0.1 M NaOH. The ionic strength of

these 2 mg mL^{-1} β-lg nanofibril samples at pH 3 was theoretically calculated to be 4.5 mM,

based on the concentrations of Na$^+$, H$^+$ and Cl$^-$ ions, excluding the contribution of any salts

that may be present in the starting material, β-lg.

For the small-angle X-ray scattering (SAXS) experiments, aliquots obtained from the

nanofibril sample prepared from 16 mg mL^{-1} β-lg solution were diluted 2-fold with pH 3 HCl,

centrifuged for the removal of macroscopic aggregates, and their pH was adjusted to 3 using

NaOH, as mentioned above. The ionic strength of this β-lg nanofibril sample at pH 3 was

theoretically calculated to be ~14 mM. Aliquots obtained from this nanofibril sample were

further diluted to 4 and 2 mg mL^{-1} using appropriate volumes of pH 3 HCl. The

concentrations given for the β-lg nanofibril samples in the following text are based on the β-lg

concentration of the initial solution subjected to nanofibril formation.

Preparation of pectin solutions

DM86 was dissolved in water to result in concentrations of 2 and 4 mg mL^{-1}. These solutions,

which had a pH of 3.2 were then adjusted to pH 3 using 1 M HCl. The 2 mg mL^{-1} DM86

solution was then diluted with appropriate volumes of pH 3 HCl to obtain concentrations of

0.4, 0.2 and 0.1 mg mL^{-1}. The DM86 solution with a concentration of 4 mg mL^{-1} was used to

introduce DM86 into β-lg nanofibril samples that had already been mixed with GalA

monomer or oligomer solutions.

In addition, DM86 was dissolved in 40 and 200 mM aqueous NaCl solutions to result

in a concentration of 2 mg mL^{-1}. The resulting solutions were further diluted with the

corresponding NaCl solution to obtain DM86 concentrations of 0.4 and 0.1 mg mL^{-1}, and then

the pH of these solutions was adjusted to 3 using 1 M HCl. These NaCl containing DM86

solutions were used when it was required to increase the ionic strength of the β-lg nanofibrils

and DM86 mixtures. Moreover, a 5 mg mL^{-1} DM86 solution was prepared in 50 mM acetate

buffer (pH 4.2) for the endo-PG digestion.

Preparation of GalA monomer and oligomer solutions

GalA monomer and oligomer stock solutions were prepared by dissolving 2.36 mg of the

monomer, or 2.58 mg of the GalA heptamer and octamer mixture respectively, accurately

measured using a METTLER AT261 DeltaRange balance (Albstadt, Germany), in 10 mL of

water. An aliquot (100 μL) obtained from each solution was then 20-fold diluted with pH 3

HCl to obtain the working solutions. The weight of the GalA monomer and the

heptamer/octamer mixture to be dissolved and the concentration of the working solutions

were predetermined based on the number of GalA monomer units expected to be present in

the final mixtures prepared with β-lg nanofibrils.

Formation of β-lg nanotapes

β-Lg nanofibril samples adjusted to pH 3 were mixed with DM86 solutions at the same pH to

result in a concentration ratio of 20:1 between β-lg nanofibrils and DM86 in the final

mixtures. ζ-Potential of CH β-lg nanofibrils, MHS β-lg nanofibrils and DM86 at pH 3 was

measured to be +40.4 ± 1.9 mV, +45.9 ± 1.6 mV and -4.2 ± 0.6, respectively.[24] The optimum

concentration ratio and pH were determined after trialling five different concentrations of

DM86 with a fixed concentration of β-lg nanofibrils at two different pH values.[24] The

resulting nanotapes had an average width of ~180 nm, up to a β-lg concentration of 20 mg

mL^{-1}.[24] The concentration of the each component used to form a mixture was twice that of the

required concentration in the final mixture (*i.e.* components were mixed in equal volumes).

The component concentrations given for the mixtures in the following text refer to their final

concentrations. pH of the individual solutions was verified to be at pH 3 before mixing.

Mixtures were kept at room temperature (~20 °C) for a minimum of 2 h before subjecting the

samples to any evaluation. pH of these prepared mixtures was 3.0 ± 0.1.

Increasing the ionic strength and the pH of nanotape forming medium

The ionic strength of the nanotape forming medium was increased by the use of DM86

solutions at pH 3 containing either 40 or 200 mM NaCl for the preparation of mixtures.

Among the prepared mixtures, 1 mg mL^{-1} CH β-lg nanofibrils + 0.05 mg mL^{-1} DM86

mixtures with 20 and 100 mM final NaCl concentrations were subjected to electron

mciroscopy to determine the effect of ionic strength on the nanotape formation.

Moreover, aliquots obtained from 1 mg mL^{-1} CH β-lg nanofibrils + 0.05 mg mL^{-1}

DM86 mixture at pH 3 were adjusted to pH 4, 6 and 7 by the addition of 0.1 and/or 0.5 M

NaOH. pH adjusted mixtures were then subjected to electron mciroscopy to determine the

effect of pH on the nanotapes.

Small-angle X-ray scattering (SAXS) experiments

 Synchrotron X-ray scattering experiments were conducted using the SAXS/WAXS beamline

of the Australian Synchrotron in Melbourne. X-rays with a wavelength of 0.1032 nm were

used, and the scattering data were collected at two camera lengths (7000 and 650 mm) using a

Pilatus 1M image plate detector. Samples were subjected to 24×1 s exposures (24 frames),

while they were flowing inside a quartz capillary cell, which were monitored for evidence of

sample damage. The cell was automatically rinsed in between samples using a sequential

series of water, surfactant, water, guanidine hydrochloride and water. Scattering data were

collected for a minimum of two concentrations of a given sample. Each sample was preceded

by its buffer (*i.e*. pH 3 HCl, or pH 3 HCl with 100 mm NaCl), and the buffer scans between

subsequent samples were compared to ensure that there was no detectable build up of aggregates on the capillary cell.

SAXS data reduction and analysis

Each of the 24 frames collected for a sample at a given concentration and at a given camera length was azimuthally averaged, corrected for the transmission and scaled to the absolute scattering intensity using the on-site ScatterBrain software to obtain 1-dimensional plots of the scattering intensity, I, against the scattering vector q, ($q = 4\pi \sin \theta/\lambda$, where 2θ is the scattering angle and λ is the wavelength of X-rays). All the I vs q plots obtained for a given sample were then averaged using the same software. The combination of the scattering data obtained at the two camera lengths, background subtraction and further analysis of scattering data were performed using the Igor reduction and analysis macros developed by Kline.[47] Igor Pro software (v.6.2.2.2 WaveMetrics, Lake Oswego, OR, USA) was used as the platform to run the above macros.

Determination of the structure factor for β-lg nanotapes

 The scattering intensity, I becomes proportional to the macroscopic differential scattering cross-section of the sample after the background subtraction, and the latter can be expressed as: $nV_p^2 (\Delta\rho)^2 S(q) P(q)$,[48] where n is the number density of particles, V_p is the volume of particles, $\Delta\rho$ is the difference in scattering length density between particles and solvent, $P(q)$ is the particle form factor (which provides information about particle size and shape) and $S(q)$ is the particle structure factor (which provides information about inter-particle correlations).

For dilute systems in which the particles are isotropically distributed, usually no structure factor is observed, and the scattering data represents the form factor alone. When the scattering data resulting from a particular system includes a structure factor in addition to the

form factor (as in the case of β-lg nanofibrils + DM86 mixture, *i.e*. β-lg nanotapes), the

structure factor alone can be obtained by dividing the scattering data by the data that

represents the form factor alone for that particular system. Therefore, the structure factor of

the above system was obtained by dividing the scattering data obtained for the CH β-lg

nanofibrils + DM86 mixture by the scattering data of CH β-lg nanofibrils (the contribution of

DM86 to the total scattering intensity was negligible).

Determination of the physical parameters of β-lg nanofibrils

SAXS data obtained for the CH and MHS β-lg nanofibrils were used to develop *ab initio* bead

models for ~10 nm sections of the nanofibrils along the length. Bead modelling was carried

out using the ATSAS software suite (v2.4, EMBL, Heidelberg, Germany)[49] and the steps

followed during the modelling are explained in Sec. 1 (ESI†).

Two-dimensional wide-angle X-ray diffraction (WAXD) experiments were performed

at the X-ray facility of the Institute of Fundamental Sciences (IFS) at Massey University,

Palmerston North, New Zealand to determine the inter-strand distance (*i.e*. distance between

adjacent β-strands within a β-sheet) and inter-sheet distance (*i.e*. distance between adjacent

β-sheets within a nanofibril) of 16 h CH and 2 h MHS β-lg nanofibrils. The method followed

for the WAXD experiments is given in Sec. 2 (ESI†).

Endo-PG digestion of DM86

Endo-PG concentrate was diluted 1:1000 with acetate buffer (50 mM; pH 4.2), and this

diluted enzyme solution was verified for its action by checking its activity against a low

methoxyl pectin, using a fully methylesterified homogalacturonan as a control (Sec. 3, ESI†).

Aliquots (240 μL) obtained from the diluted endo-PG solution were added into 1200 μL

volumes of 5 mg mL^{-1} DM86 in the acetate buffer, mixed well and allowed to stand at room

temperature (~20 °C). The ratio of mixing was equal to the ratio used during the verification

of enzyme action. At the requisite times (*i.e.* 0.5, 8, 24 h and 7 days), the action of endo-PG

was suppressed by reducing the pH of the DM86 samples to 3 through the addition of glacial

acetic acid.[50] After the pH reduction, the samples were stored at 4 °C until they were further

analysed and interacted with CH β-lg nanofibrils.

Characterisation of DM86 digest

The products resulting from the endo-PG digestion of DM86 over time were assessed for their

charge by CE. In addition, molecular weights of the products in selected samples (0.5 h, 24 h

and 7 days) were determined using SEC coupled in series MALLS and RI detectors.[46]

Interacting DM86 digest with β-lg nanofibrils

Aliquots obtained from the DM86 samples treated with endo-PG for different time periods

were diluted with pH 3 HCl to result in a DM86 concentration of 0.1 mg mL^{-1} and they were

mixed with 2 mg mL^{-1} CH β-lg nanofibril samples in a 1:1 volume ratio. These mixtures were

then subjected to electron microscopy to determine the effect of endo-PG treatment of DM86

on its ability to form nanotapes.

Blocking the DM 86 interaction sites on β-lg nanofibrils

Aliquots (1 mL) obtained from the CH β-lg nanofibril sample (2 mg mL^{-1}; pH 3) were mixed

with 1 mL of either GalA monomer or GalA oligomer in an attempt to block the DM86

interaction sites on the β-lg nanofibrils by competitive inhibition. The volumes of the added

GalA monomer and GalA oligomer stock solutions were calculated so that they had

equivalent amounts of non-methylesterifed GalA monomer units as present in 1mL of 0.1 mg

mL^{-1} DM86 solution. After leaving the mixtures for 1 h at room temperature (~20 °C), 25 μL

SM-ART-06-2015-001530

of 4 mg mL^{-1} DM86 solution at pH 3 was added to each mixture to yield a final concentration

of ~0.05 mg mL^{-1} DM86. Another set of mixtures was kept without adding DM86 to observe

the effect of GalA monomer and oligomer solutions alone on the β-lg nanofibrils.

Transmission Electron Microscopy (TEM) and Cryo-Electron Microscopy (Cryo-EM)

Two electron microscopes (Philips CM12 and Tecnai 12, Eindhoven, The Netherlands)

operating at 120 kV were used for TEM. Carbon-coated 400 mesh copper grids were glow-

discharged and placed on sample droplets for ~40 s. Each grid was then washed once with

water and stained with 20 mg mL^{-1} aqueous uranyl acetate before inserting into the

microscope.

For cryo-EM, the samples (2 μL) were applied on to glow discharged cryo grids with a

pit diameter ~1 μm, blotted for 5 s and quench frozen in liquid ethane using an automated

Vitrobot system (AIM Company BV, Brunssum, The Netherlands). Vitrified specimens were

then transferred and mounted under liquid nitrogen onto a Gatan cryo-EM grid holder and

observed using a Tecnai 12 microscope, operating at 120 kV.

Images were acquired using Gatan CCD cameras (Pleasanton, CA, USA) attached to

both microscopes and representative images shown herein were selected from 7 or more

different data sets. Both TEM and Cryo-EM image analysis were performed using the ImageJ

software (v1.43, National Institute of Health, Bethesda, MD, USA), which allowed the pixels

to be converted to nm.

Results

Increasing the ionic strength and the pH of the medium hinders β-lg nanotape formation

Under controlled conditions, lateral assembly of β-lg nanofibrils into well-aligned nanotapes occurred in the presence of DM86 (Fig 1A). Introducing NaCl into 1 mg mL^{-1} CH β-lg nanofibrils + 0.05 mg mL^{-1} DM86 mixtures at a final concentration of 20 mM did not affect the nanotape formation (Fig. 1B). However, increasing the NaCl concentration up to 100 mM considerably reduced the lateral assembly of β-lg nanofibrils into nanotapes (Fig. 1C).

Changing the pH of 1 mg mL^{-1} CH β-lg nanofibrils + 0.05 mg mL^{-1} DM86 mixtures from pH 3 to pH 4, 6 or 7 resulted in turbid solutions and the TEM images obtained on these mixtures showed individual nanofibrils in addition to clustered nanotapes (Fig. 2). The amount of individual nanofibrils observed on the grids increased with the increasing pH, while the number of nanotapes observed concomitantly reduced (Fig. 2).
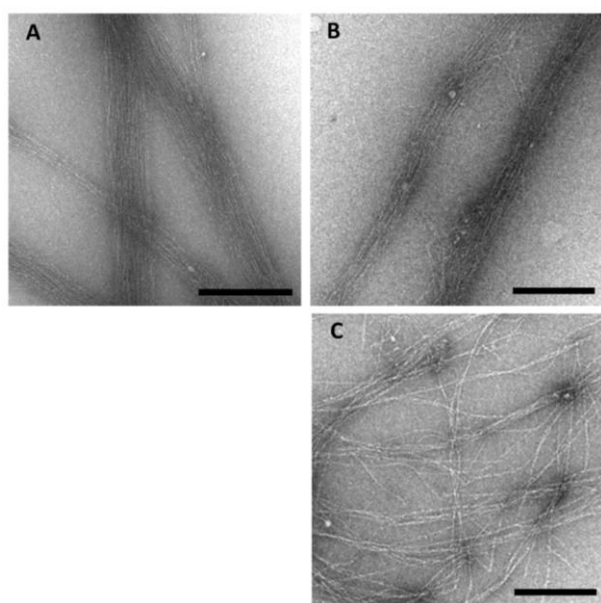
Fig. 1 TEM images obtained for 1mg mL^{-1} CH β-lg nanofibrils + 0.05 mg mL^{-1} DM86 mixtures at pH 3. (A) without addition of NaCl. (B) with 20 mM NaCl and (C) with 100 mM NaCl. Scale bars represent 0.5 μm.
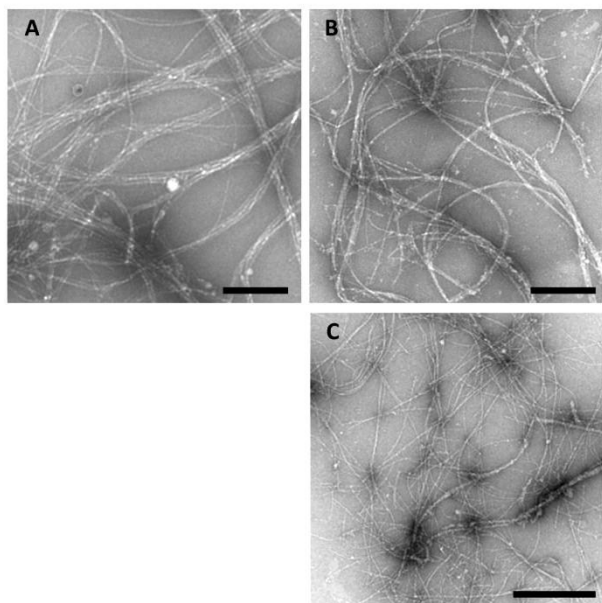
Fig. 2 TEM images obtained for 1 mg mL^{-1} CH β-lg nanofibrils + 0.05 mg mL^{-1} DM86 mixtures after increasing their pH with NaOH. (A) pH 4, (B) pH 6 and (C) pH 7. Scale bars represent 0.5 μm.

Alignment of β-lg nanofibrils within a nanotape is more relaxed under aqueous conditions

Cryo-EM images obtained for the β-lg nanotapes showed that the β-lg nanofibrils are more loosely packed within a nanotape in comparison to the highly ordered alignment shown in TEM images (Fig. 3A,B) suggesting that these nanotapes are less rigid/more flexible under aqueous conditions or that one or both of the microscopy methods introduces preparation artefacts into the images. It should also be noted that the TEM images were collected on samples dried onto a grid surface, and therefore, it is possible that the individual nanofibrils within a nanotape were forced towards each other due to the drying effects. Cryo-EM images of β-lg nanotapes were obtained under the frozen state of the sample, hence there are no drying effects as with TEM, although freezing artifacts are possible.

15

Both TEM and Cryo-EM images of β-lg nanotapes further suggested that they are

mostly made of a single layer of laterally aligned nanofibrils, with occasional stacking (some

nanotapes appeared to split into two with their progression) (Fig. 3A,B). The histogram given

in Fig. 3C presents the distribution of inter-nanofibril distances (from surface to surface of

two adjacent nanofibrils) found within CH β-lg nanotapes measured using cryo-EM images.

The highest frequency was recorded for an interval of 8–10 nm.
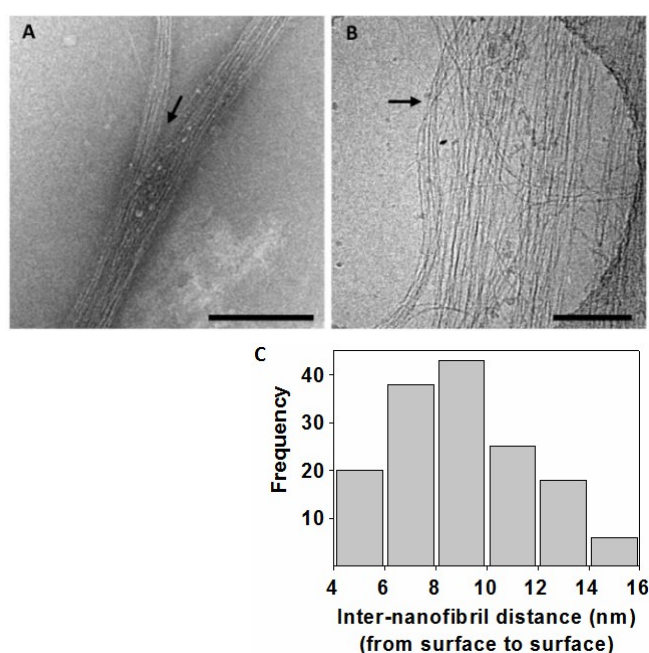
Fig. 3 Comparison of the morphology of CH β-lg nanotapes in TEM and Cryo-EM

micrographs. (A) A TEM image obtained for the 1 mg mL^{-1} CH β-lg nanofibrils + 0.05 mg

mL^{-1} DM86 mixture at pH 3. Scale bar represents 0.5 μm. (B) A Cryo-EM image obtained

for the same mixture. Scale bar represents 0.25 μm. Arrow in the image A shows a point of

splitting for a dual-layered nanotape. Arrow in the image B shows a point of twisting in a

nanotape, which essentially shows that it is made of a single layer. (C) A histogram

showing the distribution of inter-nanofibril distance (from surface to surface of two

adjacent nanofibrils) within CH β-lg nanotapes (n = 150) measured using cryo-EM images.

Additional TEM and cryo-EM images of nanotapes are given in Sec. 4 (ESI†).

Structural differences between β-lg nanofibrils and nanotapes are evident by SAXS data

Combining the SAXS data collected at two camera lengths gave a q range of ~0.02–9 nm^{-1}.

Comparison of the individual I vs q plots obtained for each frame of a given sample

confirmed that there was no observable beam damage during the measurement. Moreover, for

a given sample, normalised scattering data obtained from two concentrations was

superimposable (Sec. 4, ESI†), suggesting that no detectable inter-particle interactions (*i.e.*

aggregation or repulsion among the nanotape constituents) exist within the range of

concentrations used for these experiments.

       Fig. 4 presents the SAXS data recorded for the β-lg nanofibrils, DM86 and their

mixtures at their highest concentration trialed. Scattering patterns recorded for the samples

prepared with MHS β-lg nanofibrils were similar to those recorded for samples prepared with

CH β-lg nanofibrils.
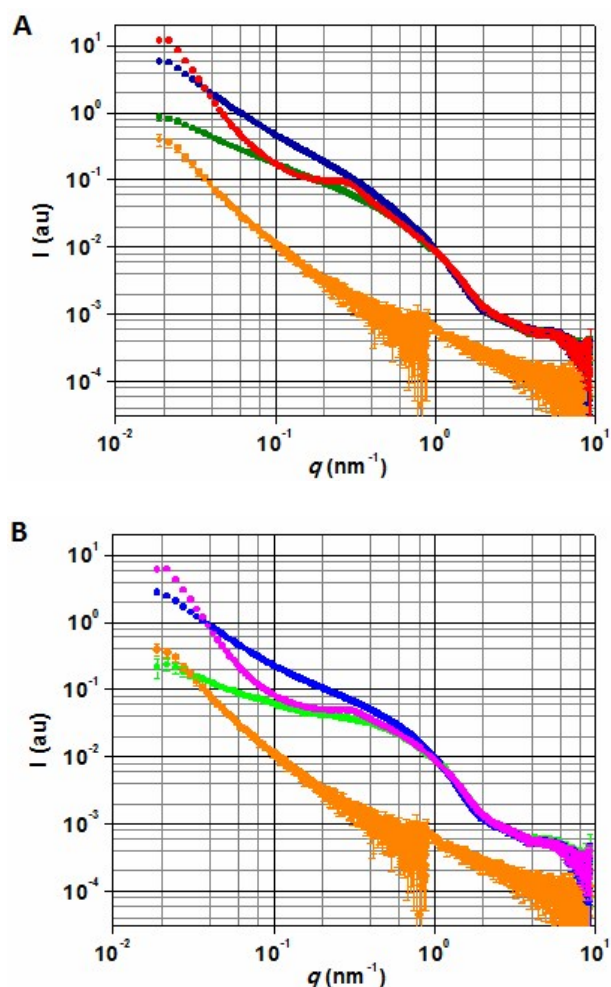
Fig. 4 Synchrotron SAXS data represented in I vs q log-log plots. (A) CH β-lg nanofibrils, DM86 and their mixtures. (B) MHS β-lg nanofibrils, DM86 and their mixtures. (●,●) 4 mg mL^{-1} β-lg nanofibrils, (●) 0.2 mg mL^{-1} DM86, (●,●) 4 mg mL^{-1} β-lg nanofibrils + 0.2 mg mL^{-1} DM86 mixture, (●,●) 4 mg mL^{-1} β-lg nanofibrils + 0.2 mg mL^{-1} DM86 mixture with 100 mM NaCl. All the samples were at pH 3.

The scattering intensity recorded for the 0.2 mg mL^{-1} DM86 sample over the experimental q range was considerably lower in comparison to the other samples. Subtraction of the scattering data of DM86 from that of the CH β-lg nanofibrils + DM 86 mixture resulted in a scattering curve that overlaid the scattering curve of the mixture within experimental uncertainties. Thus, the contribution of DM86 to the total scattering intensity of the mixture was considered to be negligible.

Scattering curves obtained for the β-lg nanofibrils + DM86 mixtures (β-lg nanotapes) were more or less identical to that of β-lg nanofibrils for $q > 0.1$ nm^{-1}, except for the presence of a peak at $q \sim 0.3$ nm^{-1}, which suggested the presence of a structure factor. Upturns in the scattering curves of β-lg nanotapes were observed at $q < 0.1$ nm^{-1}, where the data followed a power law with an exponent of -3.5±1. Scattering curves obtained for the β-lg nanofibrils + DM86 mixtures with 100 mM NaCl overlaid the scattering curves of β-lg nanofibrils up to $q \sim$ 0.8 nm^{-1}. At $q < 0.8$ nm^{-1}, a higher slope was observed for these mixtures in comparison to β-lg nanofibrils. However, no peaks were observed for these mixtures containing 100 mM NaCl, in contrast to β-lg nanotapes (Fig. 4).

Fig. 5 presents the structure factors obtained for the CH and MHS β-lg nanotapes (at the highest concentration trailed), with a peak centered at $q \sim 0.3$ nm^{-1} for both samples. The structure factor peak observed for the MHS β-lg was less intense and broader in comparison to that of CH β-lg nanotapes. Structure factor peaks observed for both CH and MHS β-lg nanotapes were fitted with the Gaussian peak model given in Igor analysis macros[47] (Fig. 5-Insets), and the parameters obtained from curve fitting are given in Table 1.
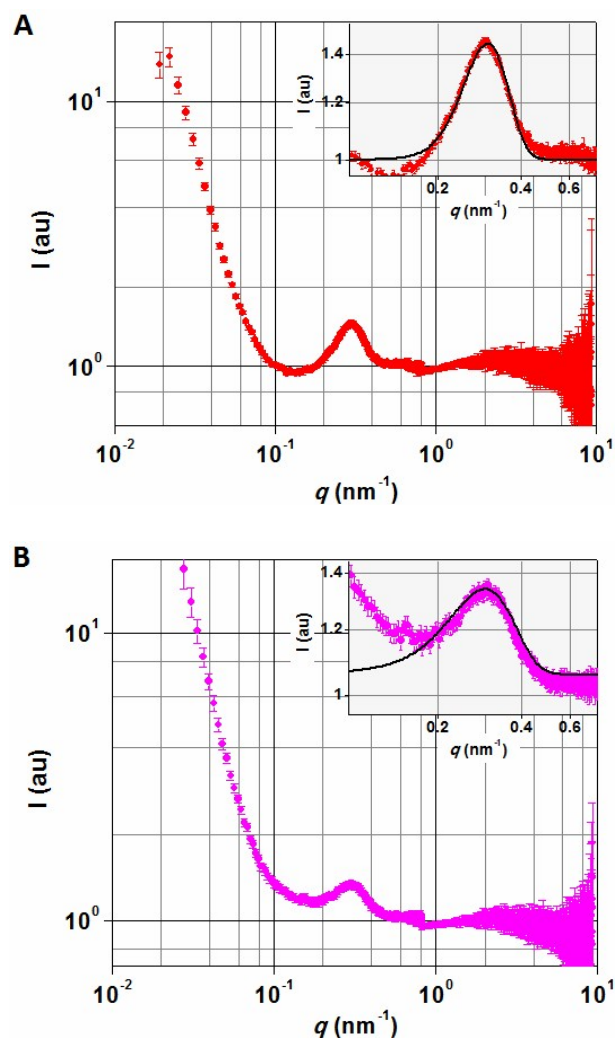
Fig. 5 Structure factor of β-lg nanotapes. (A) CH β-lg nanotapes. (B) MHS β-lg nanotapes. SAXS curve of 4 mg mL^{-1} β-lg nanofibrils + 0.2 mg mL^{-1} DM86 mixture was divided by that of 4 mg mL^{-1} β-lg nanofibrils to obtain the structure factor alone for both CH and MHS β-lg nanotapes. Insets show the structure factor peaks fitted with the Gaussian peak model (in black continuous lines).

SM-ART-06-2015-001530

Table 1 Parameters obtained for the structure factor of β-lg nanotapes by Gaussian

peak fitting

	CH β-lg nanotapes[a]	MHS β-lg nanotapes[a]
Peak position (nm^{-1})	0.30±0.05	0.30±0.07
FWHM[b] (nm^{-1})	0.13	0.16
Incoherent background	1.00	1.06

[a]Concentration of β-lg nanofibrils in the mixture was 4 mg mL^{-1}.

[b]Full width at half maximum of the scattering intensity of peak.

The distribution of non-methylesterified GalA units in the backbone of DM86 can be assessed by examining the products resulting from its Endo-PG digestion

 In order to specifically cleave any blocks of non-methylesterified GalA units that may be

present in DM86, it was treated with endo-PG, and the products resulting from digestion were

tracked over time using CE and SEC. The endo-PG treatment of a high DM pectin of random

intramolecular charge distribution would yield products broadly of two kinds, 1) small non-

methylesterified or partially methylesterified oligomers removed from regions of non-

methylesterified enzyme susceptible regions and 2) significantly longer methyl-protected

regions of the polymer containing no endo-PG-attackable motifs.

In CE experiments, the electrophoretic mobility of galacturonides with degrees of

polymerization (DP) in excess of around 20 residues is known to be dependent largely on the

average charge density, while the migration behaviour of smaller fragments depends on the

charge density and the DP.[51] Comparing the migration and thus DM of the larger fragments resulting from 0.5 h to 7 days of endo-PG digestion of DM86, a slightly higher DM was found in comparison to the original DM86 sample (Fig. 6), and consistent with this there were indications of the removal of some small fragments (sharper peaks to the right). In addition, the molecular weights of the samples measured at different times after the endo-PG treatment were found to be approximately half of the molecular weight of the original DM86 (Fig. 7). No significant differences were observed either in the migration times or the molecular weights of resulting products when the digestion time was increased beyond 7 days.
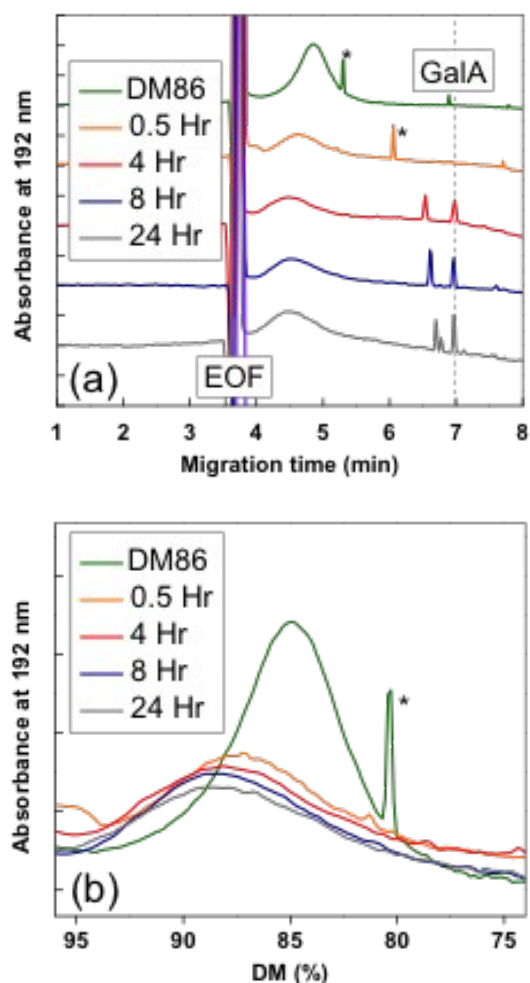
Fig. 6 Electrophorograms obtained by CE for the products resulting from endo-PG digestion

of DM86 over the time. (●) DM86 control, (●) 0.5 h, (●) 4 h, (●) 8 h, (●) 24 h. (A) shows the

whole electrophorograms: the peaks marked '*' are due to unknown particulate scattering

contaminants (they were also observed at other wavelengths when a diode array detector was

used). (B) shows the first part of the electrophorogram with their X-axes converted to DM.

The peaks observed after 6 min of elution are thought to originate from the formation of

GalA, and potentially partially methylesterified oligomers during the digestion. The dotted

line in (A) shows the expected position of monomeric galacturonic acid based on its known

electrophoretic mobility. A control electrophorogram obtained for the endo-PG solution did

not contain any peaks (not shown).
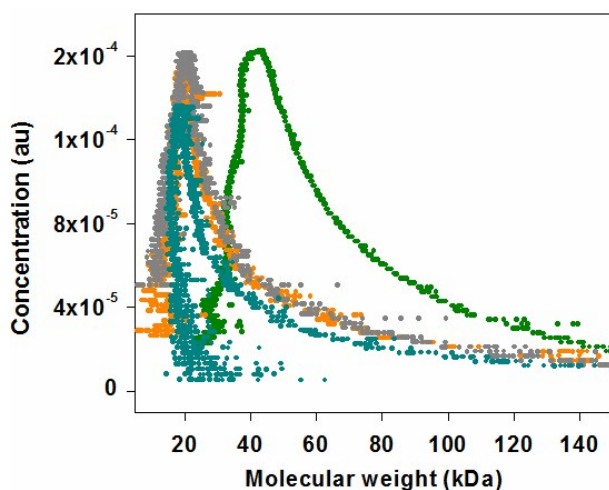
Fig. 7 Molecular weight distributions derived from LS and RI signals of SEC-MALLS for the products resulting from endo-PG digestion of DM86 over the time. (●) DM86 control, (●) 0.5 h, (●) 24 h and (●) 7 days. Average molecular weights estimated for these samples were 46.0, 23.8, 23.8 and 23.4 kDa, respectively. No peaks were observed in the LS and RI signals obtained for the endo-PG control (not shown).

Products resulting from 0.5 h to 24 h of endo-PG digestion of DM86 retained the ability to laterally assemble β-lg nanofibrils into nanotapes as shown by TEM images (Fig. 8). However, extending the endo-PG digestion period up to 7 days resulted in products that lacked the ability to form nanotapes (Fig. 8).
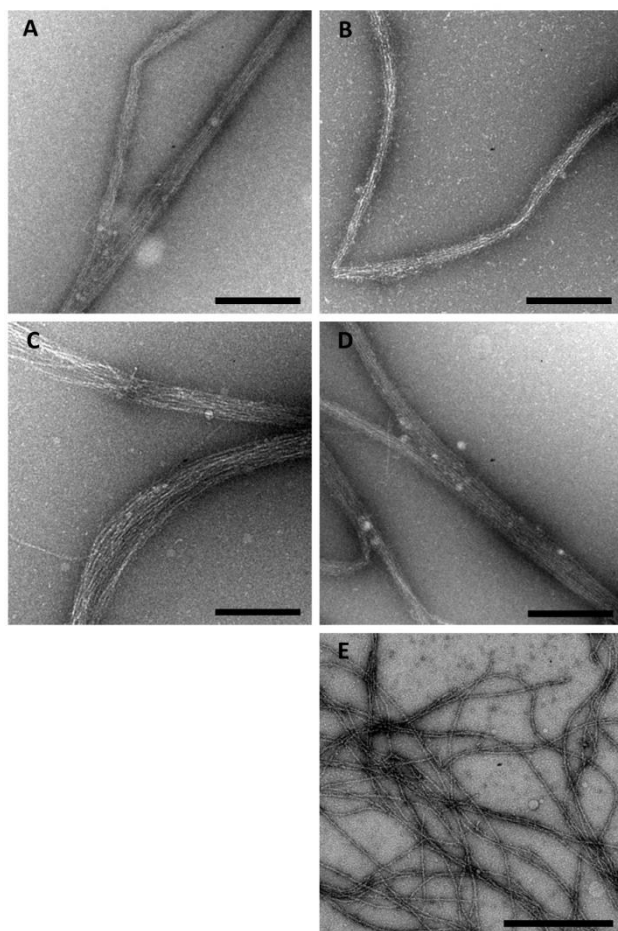
Fig. 8 TEM images obtained for the mixtures made by interacting the products resulted from endo-PG digestion of DM86 with CH β-lg nanofibrils. Duration of the endo-PG digestion of DM86 was (A) 0.5 h, (B) 4 h, (C) 8 h, (D) 24 h and (E) 7 days. Final concentrations of CH β-lg nanofibrils and endo-PG treated DM86 in the mixtures were 1 mg mL^{-1} and 0.05 mg mL^{-1}, respectively. All the mixtures had a pH of 3. Scale bars represent 0.5 μm.

Pre-incubation of β-lg nanofibrils with GalA oligomers prevents their assembly into nanotapes with DM86

In order to investigate whether the DM86 interaction sites on the nanofibrils could be competitively inhibited, they were allowed to interact with non-methylesterified GalA monomers, or a mixture of GalA heptamers and octamers, prior to pectin addition. TEM

images obtained after the simple addition of these potential inhibitors did not show any significant difference from those of β-lg nanofibrils alone (Sec. 5, ESI†). The subsequent addition of DM86 to these samples clearly showed that the GalA oligomer mixture is capable of hindering nanotape formation, as shown by free, individual nanofibrils in the TEM images acquired for this mixture, in contrast to the nanotape-forming mixture without the added oligomers (Fig. 9). Incubating β-lg nanofibrils with GalA monomers however did not affect the nanotape formation (Fig. 9).
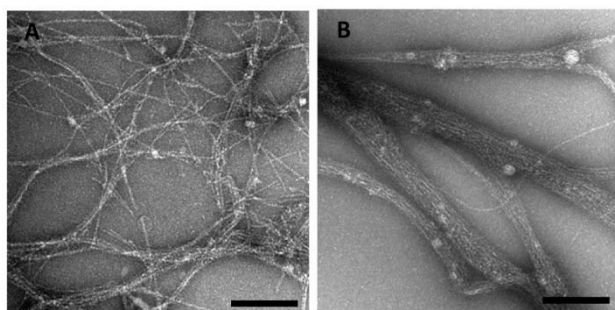
Fig. 9 TEM images showing the effect of interacting CH β-lg nanofibrils with GalA monomer and GalA heptamer and octamer mixture and subsequently with DM86 at pH 3. (A) 1 mg mL^{-1} β-lg nanofibrils + GalA oligomers + 0.05 mg mL^{-1} DM86. (B) 1 mg mL^{-1} CH β-lg nanofibrils + GalA monomers +0.05 mg mL^{-1} DM86.The final concentrations of GalA oligomer mixture and GalA monomer added to the nanofibrils were equivalent to the concentration of non-methylesterified GalA units present in DM86 at 0.05 mg mL^{-1} concentration. Scale bars represent 0.5 μm.

Discussion

To affirm the role of electrostatic interactions on the cross-linking of β-lg nanofibrils into nanotapes, the ionic strength of the β-lg nanofibrils + DM86 mixture was increased by the introduction of NaCl to final concentrations of 20 and 100 mM. Although there was no significant impact on the nanotape formation at 20 mM NaCl, increasing the NaCl concentration to 100 mM suppressed the nanotape formation (Fig. 1). This was attributed to the shielding of charges present on both DM86 molecules and on the surface of β-lg nanofibrils, which reduced the binding of DM86 molecules to the nanofibril surface and consequently prevented the linking of adjacent nanofibrils. In agreement, Sperber *et al.*[42,43] have previously shown that the binding of high-methoxyl pectins (DM ~70%) to native β-lg can be inhibited by increasing the ionic strength to 75 mM, irrespective of distribution of non-methylesterified GalA residues within the pectin molecule.

Further supporting the above hypothesis, it was found that changing the pH of the β-lg nanofibrils + DM86 mixture from pH 3 to 4, 6 and 7 also led to the gradual disassembly of nanotapes (Fig. 2). Increasing the pH of the medium reduces the net positive charge on the nanofibril surface, decreasing its affinity for the DM86 molecules.

SAXS data collected for the β-lg nanotapes revealed further information about their structure. The ordered, lateral alignment of β-lg nanofibrils within the nanotapes resulted in a structure factor peak for β-lg nanofibrils+DM86 mixtures. It is noteworthy that this structure factor does not result from nanotape-nanotape associations, in which case the peak would have been considerably more intense at the higher concentration. Such a difference in the structure factor peak intensities was not seen in the SAXS data collected for the β-lg nanotapes at two concentrations (Sec. 4, ESI†), and the observed structure factor could be safely assumed to originate from intra-fibril associations within the nanotapes. This hypothesis was further supported by the absence of any structure factor peaks in the SAXS

data recorded for the β-lg nanofibrils + DM86 mixture with 100 mM NaCl (Fig. 4), in which the nanotape formation was markedly suppressed (Fig. 1). The q value at the center of the structure factor peak of both CH and MHS β-lg nanotapes was ~0.3 nm^{-1}, and relates to a repeating distance of ~21 nm according to Bragg's law ($\lambda = 2D \sin \theta$, and $D = 2\pi/q$, where D is the repeating distance). This value was considered as the repeating distance between the central axes of two adjacent β-lg nanofibrils within a nanotape.

The structure factor peaks originating from both the CH and MHS β-lg nanotapes were found to be broader than expected for a well-aligned three dimensional lattice, suggesting that the tapes do not consist of multiple layers of nanofibrils. Moreover, if the nanotapes were predominantly made of multiple layers that were arranged in either parallel or slipped planes, another structure factor corresponding to a distance of $\sqrt{2}D$ or $\sqrt{3}D$ (*i.e.* the diagonal distance) would be present in the SAXS data (Sec. 6, ESI†). In agreement with the SAXS results, TEM and cryo-EM images obtained for the nanotapes did indicate that fibrils mainly consist of either a single layer or at most dual layers (Fig. 3).

At $q < 0.1$ nm^{-1}, the scattering curves obtained for CH or MHS β-lg nanotapes did not superimpose with the scattering curves obtained from the respective constituent β-lg nanofibrils (Fig. 4), suggesting the possibility of structural differences between nanofibrils and nanotapes at larger length scales. According to the TEM images, β-lg nanotapes exhibited a lower flexibility (a higher persistence length, l_p) in comparison to individual nanofibrils (Sec. 7, ESI†). Moreover, the contour length, l_c , of the nanotapes was higher than that of individual nanofibrils that usually average around 5 μm.[30,33,34] Indeed, the low magnification TEM images obtained for the CH β-lg nanotapes clearly showed that the l_c of the nanotapes easily exceeds 20 μm (Sec. 7, ESI†).

Modelling of the SAXS data for the region of 0.3–2.0 nm^{-1} resulted in elongated, rod-like bead models for both the CH and MHS β-lg nanofibrils (Sec. 1, ESI†). The cross-

sectional diameter of these model scatterers was ~ 3.5 nm, which is significantly smaller than the diameter of β-lg nanofibrils, (found to range from 6 to 15 nm for both CH and MHS β-lg nanofibrils (Sec. 8, ESI†), suggesting that the scattering at this length scale actually originates from protofilaments, which are the primary units that assemble into β-lg nanofibrils. Moreover, the half pitch (½ P) of these models appeared to be well below the values reported for β-lg nanofibrils by Arnaudov et al.[52] (½ P ~26 nm) and Adamcik et al.[30] (½ P ≥ 18 nm) (Sec. 1, ESI†), further suggesting that the *ab initio* models represent the protofilaments.

Zooming in further, two dimensional WAXD experiments conducted on both CH and MHS β-lg nanofibril samples showed reflections corresponding to distances of 0.47 and 1.1 nm (Sec. 2, ESI†) in agreement with previous work of Gosal et al.[53] and Bromley et al.[54] These reflections are typical of amyloid fibrils,[55] and represent the inter-strand (within a β-sheet) and inter-sheet (within a protofilament) distances respectively. Comparison of the inter-sheet distance with the diameter of a β-lg protofilament suggested that each protofilament is made of 4 β-sheets, irrespective of the method of β-lg nanofibril formation. Arrangement of these 4 β-sheets with an inter-sheet distance of 1.1 nm results in a total distance of 3.3 nm between the first and fourth, comparable to the diameter of a protofilament (~3.5 nm).

If 3.5 nm is indeed taken as the typical diameter of a β-lg protofilament, then intact β-lg nanofibrils made of 2 or 3 protofilaments would have diameters of ~7 nm or 10.5 nm respectively. Based on AFM height measurements Adamcik et al.[30] reported a diameter of 2 nm for the β-lg protofilaments, and diameters of 4 and 6 nm for β-lg nanofibrils made of 2 and 3 protofilaments respectively. However, it should be noted that the diameters obtained for protofilaments and nanofibrils by AFM could be lower owing to compression by the AFM tip during the measurements. In agreement with this suggestion, Gosal et al.[56] estimated an average diameter of 8.5 nm for the β-lg nanofibrils by TEM, while AFM gave a diameter of 3.6 nm.

SM-ART-06-2015-001530

Taking the diameter of individual β-lg nanofibrils estimated from the *ab initio*

models, together with the distance between the central axes of adjacent nanofibrils within a

nanotape as determined by the *q* value of the structure factor peak then the distance between

the surfaces of adjacent nanofibrils can be calculated. If the adjacent β-lg nanofibrils were

made of 2 protofilaments, the space available between the surfaces of the nanofibrils would be

~14 nm. Alternatively, if the adjacent β-lg nanofibrils were made of 3 protofilaments, the

space between the surfaces would be ~10.5 nm. These values are consistent with the results of

cryo-EM image analysis, which gave a distribution for the space between the surfaces of two

adjacent nanofibrils with a range 4–16 nm and a maximum at ~ 8–10 nm. There is, therefore,

adequate space available for the DM86 molecules to sandwich in between two adjacent

nanofibrils within a nanotape, consistent with the hypothesis that DM86 molecules indeed

cross-link the β-lg nanofibrils.

The structure factor peak observed for the MHS β-lg nanotapes had a lower intensity

in comparison to that of CH β-lg nanotapes (Fig. 5). This may be simply due to differences in

the relative concentrations of nanofibrils and nanotapes for CH and MHS β-lg. Otherwise, it

suggests that the individual nanofibrils within MHS β-lg nanotapes exist in a less ordered

fashion. Given the distance between the surfaces of adjacent nanofibrils, it is unlikely that

protrusions, reported to be present on the surface of MHS β-lg nanofibrils[29] significantly

affect the packing of nanofibrils as the length of these protrusions are comparatively small.

However, the amount of DM86 molecules that could potentially bind with protrusion-rich

MHS β-lg nanofibrils may be higher than the amount that can bind with CH β-lg nanofibrils,

affecting their alignment. Indeed, in other work we found that MHS β-lg nanofibrils do tend

to bind with more pectins than CH β-lg nanofibrils,[24] supporting this idea.

As it was evident that electrostatic interactions play an important role in the formation

of nanotapes, efforts were made to understand the distribution of the limited number of

negatively charged, non-methylesterified GalA residues within the backbone of the DM86

molecules. According to calculations based on the M_w, GalA content and DM, a

representative average backbone might be thought of as consisting of ~224 GalA residues

with ~192 of these methylesterified. In concert with previous evidence, homogalacturonan

blocks generally appear rather monodisperse with a DP of around 100 residues.[57] It is

possible that a short rhamnogalacturonan-I section might also be present, located fairly

centrally along the backbone.[58] With around only ~32 potentially-charged GalA residues

along the DM86 chains, a random distribution of these moieties seems unlikely to be able to

provide the locally required negative charge density in order to create a strong electrostatic

interaction between the pectin molecules and β-lg nanofibrils. Hence, it is hypothesised that a

more block-wise distribution of non-methylesterified GalA residues might exist in DM86. In

fact, it has been previously reported that β-lg shows a higher affinity towards the pectins with

a block-wise distribution of non-methylesterified GalA residues, in comparison to those with

a random distribution.[42]

In order to test this hypothesis attempts were made to specifically remove any non-

methylesterified GalA blocks that may be present in DM86, using an endopolygalacturonase

(the endo-PG II isoform from *Aspergillus niger*). The binding site of the endo-PG consists of

4 main subsites and the enzyme needs a block containing a minimum of 3, but preferably 4

non-methylesterified GalA residues to bind and perform chain cleavage.[59] Polygalacturonic

acid (PGA) is quickly digested to the monomer, dimer and trimer by this enzyme.

Trigalacturonic acid can itself be digested albeit at a considerably slower rate than the

tetramer. Cleavage within the trimer always occurs between the last 2 residues at the reducing

end of the enzyme-bound part of the substrate, and for all scissions there is a strict

requirement that residues on either side of the cleavage site must not be methylesterified.[59]

Blocks of non-methylesterified galacturonic acid that exist within the polymer will be

removed, and if the fragments are excised from stretches of a greater length than around 10 residues, then the relative ratios of the released monomer, dimer and trimer approaches that found for PGA but when there are less than 10 residues there are only monomers.[60]

As described above, CE experiments carried out on endo-PG treated pectins are expected to reveal two distinct characteristics 1) small non-methylesterified or partially methylesterified oligomers removed from enzyme-susceptible regions that would migrate as comparatively narrow peaks to the right (higher negative charge density) of the high DM starting material; and 2) significantly longer methyl-protected regions of the polymer containing no endo-PG-attackable motifs that would yield a wider starting-material-like peak, but potentially shifted to the left (lower negative charge density). The results shown in Fig. 6 provide strong evidence for the removal of non-methylesterified GalA residues from the DM86 backbone by the endo-PG treatment. The narrower peaks observed at migration times greater than 6 min for the DM86 samples treated with endo-PG for 4 h and beyond (Fig. 6) can be attributed to those removed non-methylesterified GalA residues, which can be present as GalA monomers, dimers, trimers, or even as small partially-methylesterified oligomers.[44,59,61] Aligning the most significant peak of each electrophorogram in this region and assuming that it represents a single substance showed that the intensity of this peak gradually increases with the duration of the endo-PG treatment, and gives an electrophoretic mobility consistent with the GalA monomer. The absence of clear peaks for di- and tri-galacturonic acids, and in particular the lack of relative amounts consistent with the results of PGA fragmentation suggests that these fragments were predominantly excised from blocks that were smaller than 10 residues.

SEC-MALLS results showed that the methylester-protected products (also observed in CE as starting-material-like peaks of slightly higher DM) had a M_w of ~23 kDa, approximately half of the M_w of the original undigested DM86 (~48 kDa) (Fig. 7). Taken at

face value this suggests that the starting substrate carries enzyme susceptible motifs of non-methylesterified GalA residues approximately in the middle of the homogalacturonan backbone, rather than being randomly distributed. Indeed, if any other endo-PG susceptible blocks of non-methylesterified GalA residues had been available in the starting DM86 molecules at any location along the backbone, the action of endo-PG would have resulted in some products with a M_w much less than half of the M_w of the original DM86.

After 7 days the resulting products of the endo-PG treatment (Figs. 6, 7) lacked the ability to form nanotapes (Fig. 8) suggesting that indeed prolonged digestion removes motifs capable of coupling the nanofibrils as hypothesised. However, while the duration of the endo-PG treatment on DM86 did not appear to have a significant effect on either the DM or the M_w of the detected products, only after 7 days was nanotape formation completely prevented. The initial action of endo-PG on DM86 therefore appears to result in two homogalacturonan chains of fairly similar size as described above, but that a good number of these additionally carry non-methylesterified GalA motifs both at the recently severed end and at opposite end, permitting some nanotape formation. Over time, trimming of the non-methylesterified GalA motifs at the ends of these chains will take place due to the action of endo-PG, and it will reduce their ability to bind with β-lg nanofibrils and to form nanotapes. However, the number of non-methylesterified GalA residues removed in this manner will be markedly lower in comparison to the total number of GalA residues present in these chains, so that no significant effect on the DM and M_w of the methylester protected chains can be measured (while there is a small increase in the CE-detected fragment peaks).

The DM of these methylester protected chains was found to be only slightly higher than DM86 even after 7 days (86 ± 2% compared to 89± 2%; Fig. 6), suggesting that a significant portion of non-methylesterified GalA residues in DM86 are still randomly distributed and unsusceptible to endo-PG attack. According to the information obtained from

the manufacturer, the high DM of this pectin has been achieved by chemical

methylesterification of a pectin with a lower degree of methylesterification, and it is therefore

entirely possible for the DM86 molecules to have a noticeable amount of non-methylesterified

GalA residues randomly distributed along its backbone, even if the starting material had some

degree of blockiness. This is consistent with the trimming of the non-methylesterified GalA

blocks described, indeed having a minimal affect on the DM as shown by the

electrophorograms (Fig. 6).

Considering the average DM and M_w of the large methylester protected chains that

resulted from initial endo-PG cleavage together with the possible endo-PG cleavage sites, the

following structural models are proposed for the DM86 backbone (Fig. 10). Calculations

performed and the assumptions made to arrive on the following models are given in Sec. 9

(ESI†).

Fig. 10 Proposed structural models for the DM86 backbone. (●) Methylesterified GalA

residues (not drawn in scale with the calculated numbers). (●) Non-methylesterified GalA

residues (drawn equally to the calculated numbers). DM86 backbone carries ~192

methylesterified GalA residues and ~32 non-methylesterified GalA residues. Among the ~32

non-methylesterified GalA residues, some are randomly distributed in singles or pairs, while

the others are in blocks of ≥ 3residues. In agreement with experimental evidence, two models

can be proposed for the DM86 backbone, and they are: (A) with 2 blocks, and (B) with 3

blocks of non-methylesterified GalA residues. The approximate number of non-

methylesterified GalA residues that can be present in each block is given with the two models.

A short rhamnogalacturonan section may exist in close proximity to the middle of the

backbone, and it is not shown in the above models.

β-Lg nanotapes were observed even with the products resulting from 24 h of endo-PG

digestion of DM86, suggesting that the motifs required to create an adequate electrostatic

potential to bind with β-lg nanofibrils are actually quite small, explaining why they take some

time to be trimmed. In a further attempt to assess the potential size of the pectin-nanofibril

electrostatic interaction sites, experiments were extended hypothesizing that it was possible to

block the DM86 interaction sites on the β-lg nanofibril surface prior to the introduction of

DM86 molecules, which would hinder nanotape formation. To competitively inhibit the

DM86 interaction sites on the surface of β-lg nanofibrils, they were first incubated with

either: a mixture of GalA heptamers and GalA octamers, or with GalA monomers prior to the

introduction of DM86. Incubating β-lg nanofibrils with GalA heptamers and octamers

hindered nanotape formation, suggesting that the oligomers are capable of blocking a

considerable amount of DM86 interacting sites on β-lg nanofibrils as would be presumed

from the proposed fine structures (Fig. 9).

The formation of a small amount of nanotapes with DM86 after incubating with GalA

heptamers and octamers was observed, revealing that a limited number of binding sites were

still available on β-lg nanofibril surface to bind with the GalA blocks in DM86 molecules.

This observation further suggests that multiple sites are available on β-lg nanofibril surface

for the binding of non-methylesterified GalA blocks in DM86, and it is not necessary to

occupy all the possible binding sites on the nanofibril surface for the formation of β-lg

nanotapes. In another perspective, heptamers and octamers may be slightly larger than the

non-methylesterified GalA blocks present in DM86, and therefore they may not be as

effective as DM86 molecules in occupying the binding sites of β-lg nanofibrils. In contrast, incubating β-lg nanofibrils with GalA monomers did not affect the nanotape formation (Fig. 9). Given the smaller size of GalA monomers their interactions are expected to be considerably more dynamic.

The ability of the GalA heptamers and octamers to retard nanotape formation provides complementary evidence for the nature of the DM86 binding motif as small block-wise sections of charged non-methylesterified GalA residues (in addition to the ionic strength and pH dependence). The ability of DM86 molecules to cross-link β-lg nanofibrils relies crucially on the binding of these negatively charged motifs with the nanofibril surface, and additionally that these binding points are separated by long methyl-protected chain sections that can act as tethers. Indeed, no nanotape formation was observed in the presence of GalA heptamers and octamers alone (Sec. 5, ESI†), revealing that the charged blocks themselves are not sufficient for the nanotape formation. Based on these facts, the following mechanism is proposed for the β-lg nanotape formation.

Non-methylesterified GalA blocks present in the DM86 backbone act as binding motifs, and they interact electrostatically with two individual β-lg nanofibrils, bridging them together. Once they are brought together, hydrogen bonding and hydrophobic interactions can also make contributions to the binding of the pectin to the nanofibrils. The methylesterified GalA blocks present in between the charged blocks act as spacers. Moreover, methylesterified GalA blocks of DM86 molecules attached to the adjacent nanofibrils, can interact hydrophobically with each other, contributing to the amalgamation of neighbouring β-lg nanofibrils. Although some non-methylesterified GalA residues can be present on these methylesterifed GalA blocks, their charge has a negligible effect on hydrophobic interactions owing to their low number and random distribution. The possibility of such pectin-pectin

hydrophobic interactions associated with the methyl groups of their GalA residues has been previously reported by Oakenfull and Scott,[62] and Evageliou *et al.*[63]

Given the size of a GalA residue is ~0.44 nm,[64] and the inter-strand distance within a β-sheet of a β-lg protofilament is ~0.47 nm (Sec. 2, ESI†) it is conceivable that the carboxyl groups in a block of non-methylesterified GalA residues interact with positively charged amino acid residues present in sequential β-strands. However, it would be a challenging task to identify the exact locations of the potential interactions on each β-strand due to limitations associated with the rigid body modelling of β-lg protofilaments. Nevertheless, it can be thought that the sequential β-strands that interact with the charged blocks of DM86 molecules carry positively charged amino acid residues in a roughly parallel alignment to facilitate the binding of the charged blocks.

Conclusion

β-Lg nanofibrils formed by both CH and MHS methods can be laterally aligned into ordered nanotapes, optimally at pH 3, by the use of specific highly methylesterified pectins. Cross-linking pectins should have a high DM (~86%), with a proportion of their non-methylesterified galacturonic acid residues arranged into blocks. While these blocks act as localised electrostatic binding motifs they should be separated by methyl-protected regions long enough to act as inter-nanofibril tethers. Electrostatic interactions between the negatively charged blocks and positively charged amino acid residues present in β-lg nanofibrils are essential for nanotape formation, while hydrophobic interactions between methylesterified GalA residues may also play a role in stabilizing these nanoarchitectures.

Acknowledgements

References

1. D. Stock, K. Namba and L. K. Lee, *Curr. Opin. Biotechnol.*, 2012, **23**, 545−554.

2. S. Tonddast-Navaei and G. Stan, *J. Am. Chem. Soc.*, 2013, **135**, 14627−14636.

3. X. Ye and G. H. Lorimer, *Proc. Natl. Acad. Sci. U. S. A.*, 2013, **110**, E4289−E4297.

4. J. Zheng, A. Jiao, R. Yang, H. Li, J. Li, M. Shi, C. Ma, Y. Jiang, L. Deng and W. Tan, *J. Am. Chem. Soc.*, 2012, **134**, 19957−19960.

5. J.-W. Oh, W.-J Chung, K. Heo, H.-E. Jin, B. Y. Lee, E. Wang, C. Zueger, W. Wong, J. Meyer, C. Kim, S.-Y. Lee, W.-G. Kim, M. Zemla, M. Auer, A. Hexemer and S.-W. Lee, *Nat. Commun.*, 2014, 5.

6. G. R. Heath, R. H. Abou-Saleh, S. A. Peyman, B. R. G. Johnson, S. D. Connell and S. D. Evans, *Soft Matter*, 2014, **10**, 694−700.

7. J. Wu and J. C. Meredith, *ACS Macro Lett.*, 2014, **3**, 185−190.

8. Y. Zhao, T. Ji, H. Wang, S. Li, Y. Zhao and G. Nie, *J. Controlled Release*, 2014, **177**, 11−19.

9. D. J. McGillivray, G. Valincius, D. J. Vanderah, W. Febo-Ayala, J. T. Woodward, F. Heinrich, J. J. Kasianowicz and M. Lösche, *Biointerphases*, 2007, **2**, 21–33.

10. N. Sancho Oltra, W. R.Browne, and G. Roelfes, *Chem. Eur. J.*, 2013, **19**, 2457–2461.

11. S. M. Loveday, X. L. Wang, M. A. Rao, S. G. Anema, L. K. Creamer and H. Singh, *Int. Dairy J.*, 2010, **20**, 571−579.

12. J. Adamcik and R. Mezzenga, *Soft Matter*, 2011, **7**, 5437–5443.

13. L. J. Domigan, J. P. Healy, S. J. Meade, R. J. Blaikie and J. A. Gerrard, *Biopolymers*, 2012, **97**, 123–133.

14. S. M. Loveday, X. L. Wang, M. A. Rao, S. G. Anema and H. Singh, *Food Hydrocolloids*, 2012, **27**, 242–249.

15. T. P. J. Knowles, T. W. Oppenheim, A. K. Buell, D. Y. Chirgadze and M. E. Welland, *Nat. Nanotechnol.*, 2010, **5**, 204−207.

16. S. M. Pilkington, S. J. Roberts, S. J. Meade and J. A. Gerrard, *Biotechnol. Prog.*, 2010, **26**, 93−100.

17. S. P. Rao, S. J. Meade, J. P. Healy, K. H. Sutton, N. G. Larsen, M. P. Staiger and J. A. Gerrard, *Biotechnol. Prog.*, 2012, **28**, 248−256.

18. C. Li and R. Mezzenga, *Nanoscale*, 2013, **5**, 6207−6218.

19. U. Shimanovich, I. Efimov, T. O. Mason, P. Falgmeier, A. K. Buell, A. Gedanken, S. Linse, K. S. Åkerfeldt, C. M. Dobson, D. A. Weitz and T. P. J. Knowles, *ACS Nano*, 2015, **9**, 43–51.

20. D. M. Ridgley, E.C. Claunch, P.W. Parker and J. R. Barone, *Biomacromolecules*, 2014, **15**, 1240−1247.

Soft Matter Accepted Manuscript

21. D. M. Ridgley, B.G. Freedman, P.W. Lee and J. R. Barone, *Biomater. Sci.*, 2014, **2**, 560−566.

22. E. Frare, P. P. De Laureto, J. Zurdo, C. M. Dobson and A. Fontana, *J. Mol. Biol.*, 2004, **340**, 1153−1165.

23. C. Akkermans, P. Venema, A. J. Van Der Goot, H. Gruppen, E. J. Bakx, R. M. Boom and E. Van Der Linden, *Biomacromolecules*, 2008, **9**, 1474−1479.

24. C. A. Hettiarachchi, beta-Lactoglobulin Nanofibrils and their Interactions with Pectins, Ph.D. Thesis, University of Auckland, 2013.

25. S. Brownlow, J. H. M. Cabral, R. Cooper, D. R. Flower, S. J. Yewdall, I. Polikarpov, A. C. T. North and L. Sawyer, *Structure*, 1997, **5**, 481−495.

26. D. Mercadante, L. D. Melton, G. E. Norris, T. S. Loo, M. A. K. Williams, R. C. J. Dobson and G. B. Jameson, *Biophys*. *J*., 2012, **103**, 303−312.

27. S. G. Bolder, A. J. Vasbinder, L. M. C. Sagis and E. Van Der Linden, *Int*. *Dairy J*., 2007, **17**, 846−853.

28. C. Lara, J. Adamcik, S. Jordens and R. Mezzenga, *Biomacromolecules*, 2011, **12**, 1868−1875.

29. C. A. Hettiarachchi, L. D. Melton, J. A.Gerrard and S. M. Loveday, *Biomacromolecules*, 2012, **13**, 2868−2880.

30. J. Adamcik, J.-M. Jung, J. Flakowski, P. De Los Rios, G. Dietler and R. Mezzenga, *Nat*. *Nanotechnol*., 2010, **5**, 423−428.

31. S. Bolisetty, J. Adamcik and R. Mezzenga, *Soft Matter*, 2011, **7**, 493−499.

32. P. Aymard, T. Nicolai, D. Durand and A. Clark, *Macromolecules*, 1999, **32**, 2542−2552.

33. L. M. C. Sagis, C. Veerman and E. Van Der Linden, *Langmuir*, 2004, **20**, 924−927.

34. S. S. Rogers, P. Venema, L. M. C. Sagis, E. Van Der Linden and A. M. Donald, *Macromolecules*, 2005, **38**, 2948−2958.

35. O. G. Jones, S. Handschin, J. Adamcik, L. Harnau, S. Bolisetty and R. Mezzenga, *Biomacromolecules*, 2011, **12**, 3056−3065.

36. A. Kroes-Nijboer, H. Sawalha, P. Venema, A. Bot, E. Floter, R. Den Adel, W. G. Bouwman and E.Van Der Linden, *Faraday Discuss*., 2012, **158**, 125−138.

37. H. V. Scheller, J. K. Jensen, S. O. Sørensen, J. Harholt and N.Geshi, *Physiol*. *Plant*., 2007, **129**, 283−295.

38. G. Limberg, R. Körner, H. C. Buchholt, T. M. I. E.Christensen, P. Roepstorff and J. D. Mikkelsen, *Carbohydr*. *Res*., 2000, **327**, 293−307.

39. J. A. E. Benen, J.-P. Vincken and G.-J. W. M. Van Alebeek, in *Pectins and Their Manipulations*, ed. G. B. Seymour and J. P. Knox, CRC Press, Boca Raton, 2002, pp. 209−211.

40. E. F. Jansen and R. Jang, *J*. *Am*. *Chem*. *Soc*., 1946, **68**, 1475−1477.

41. P. Matricardi, M. Dentini, V. Crescenzi and S. B. Ross-Murphy, *Carbohydr*. *Polym*., 1995, **27**, 215−220.

42. B. L. H. M. Sperber, M. A. Cohen Stuart, H. A. Schols, A. G. J. Voragen and W. Norde, *Biomacromolecules*, 2009, **10**, 3246−3252.

43. B. L. H. M. Sperber, H. A. Schols, M. A. Cohen Stuart, W. Norde and A. G. J. Voragen, *Food Hydrocolloids*, 2009, **23**, 765−772.

44. P. J. H. Daas, K. Meyer-Hansen, H. A. Schols, G. A. De Ruiter and A. G. J. Voragen, *Carbohydr*. *Res*., 1999, **318**, 135−145.

45. R. Körner, G. Limberg, T. M. I. E. Christensen, J. D. Mikkelsen and P. Roepstorff, *Anal*. *Chem*., 1999, **71**, 1421−1427.

46. M. A. K. Williams, A. l. Cucheval, A. Ström and M.-C. Ralet, *Biomacromolecules*, 2009, **10**, 1523−1531.

47. S. Kline, *J. Appl. Crystallogr.*, 2006, **39**, 895−900.

48. A. J. Jackson, *Introduction to Small-Angle Neutron Scattering and Neutron Reflectometry*, NIST Center for Neutron Research, Gaithersburg, 2008, p. 12.

49. M. V. Petoukhov, D. Franke, A. V. Shkumatov, G. Tria, A. G. Kikhney, M. Gajda, C. Gorba, H. D. T. Mertens, P. V. Konarev and D. I. Svergun, *J. Appl. Crystallogr.*, 2012, **45**, 342−350.

50. J. A. E. Benen, H. C. M. Kester and J. Visser, *Eur. J. Biochem.*, 1999, **259**, 577−585.

51. M. A. K. Williams, T. J. Foster and H. A. Schols, *J. Agric. Food Chem.*, 2003, **51**, 1777−1781.

52. L. N. Arnaudov, R. De Vries, H. Ippel and C. P. M. Van Mierlo, *Biomacromolecules*, 2003, **4**, 1614−1622.

53. W. S. Gosal, A. H. Clark and S. B. Ross-Murphy, *Biomacromolecules*, 2004, **5**, 2430−2438.

54. E. H. C. Bromley, M. R. H. Krebs and A. M. Donald, *Faraday Discuss.*, 2005, **128**, 13−27.

55. M. Sunde and C. Blake, in *Advances in Protein Chemistry*, ed. F. M. Richards, D. S. Eisenberg and P. S. Kim, Academic Press, New York, 1997, pp. 123−159.

56. W. S. Gosal, A. H. Clark, P. D. A. Pudney and S. B. Ross-Murphy, *Langmuir*, 2002, **18**, 7174−7181.

57. P. Hellín, M.-C. Ralet, E. Bonnin and J.-F. Thibault, *Carbohydr. Polym.*, 2005, **60**, 307−317.

58. B. M. Yapo, P. Lerouge, J.-F. Thibault and M.-C. Ralet, *Carbohydr. Polym.*, 2007, **69**, 426−435.

SM-ART-06-2015-001530

59. Ľ. Rexová-Benková, *Eur. J. Biochem.*, 1973, **39**, 109−115.

60. M. A. K. Williams, A. Cucheval, A. T. Nasseri and M.-C. Ralet, *Biomacromolecules*, 2010, **11**, 1667−1675.

61. P. J. H. Daas, A. G. J. Voragen and H. A. Schols, *Carbohydr. Res.*, 2000, **326**, 120−129.

62. D. Oakenfull and A. Scott, *J. Food Sci.*, 1984, **49**, 1093−1098.

63. V. Evageliou, R. K. Richardson and E. R. Morris, *Carbohydr. Polym.*, 2000, **42**, 245−259.

64. S. Cros, C. H. Du Penhoat, N. Bouchemal, H. Ohassan, A. Imberty and S. Pérez, *Int. J. Biol. Macromol.*, 1992, **14**, 313−320.